CrossMark

ORIGINAL ARTICLE

On the movement of tropical cyclone LEHAR

Hari Prasad Dasari[1] · Brahmananda Rao V[2,3] · Ramakrishna SSVS[2] ·
Paparao Gunta[2] · Nanaji Rao N[2] · Ramesh Kumar P[2]

Abstract

Purpose In this paper, an attempt has been made to delineate the physical processes which lead to the westward movement of the North Indian Ocean tropical cyclone LEHAR.

Methods The Advanced Weather Research and Forecasting (ARW) model is used to simulate LEHAR with 27 and 9 km resolutions. In addition to that, all terms of the complete vorticity equation are computed to obtain the contribution of each term for the vorticity tendency. The vorticity tendency is calculated in four sectors, namely northwest, northeast, southwest, and southeast and assumed that the cyclone moves from its existing location to the nearest point where the vortices tendency is maximum.

Results The results indicate that the model performed well in simulating the characteristics of cyclone compared with the Satellite and other observations. It is noticed that the vorticity stretching term contributes most to the positive vorticity tendency. The second highest contribution is from the horizontal advection thus indicating the secondary importance of steering.

Conclusions The distribution of lightning flash rates are higher in the SW and followed by NW sectors of the cyclone indicate more strong convective clouds are in SW sector. The equivalent potential temperatures (θ_e) at different stages of before, during and after the mature stage of the cyclone reveals that the wind-induced surface heat (WISH) exchange process is a plausible mechanism for the intensification of LEHAR.

Keywords Tropical cyclone · North Indian ocean · Westward movement · Vorticity tendency · Lightening flashes

1 Introduction

Prediction of the movement of the tropical cyclone is a very important issue for the policy makers to take necessary precautions to minimize the damaging cost and related human deaths due to storm surge, gale winds and torrential rains. The dynamics of tropical cyclone and their movement is explained by several studies. The atmospheric vortices such as tropical cyclone propagation was first explained by Rossby (1948) and he examined the motion of a rigid body rotation vortex on a beta plane in a resting environment. The first correct approximate solution was obtained by Adem (1956) by solving the non-divergent, barotropic vorticity equation. In this the variations in the coriolis force, known as a beta drift, moves westward and poleward of the cyclone embedded in the resting atmosphere. Chan and Williams (1987) and Smith (1993) showed with the numerical simulations that the meridional beta drift displacement decreases by about 45% when the vortex moves from 10 to 30°N indicating that the cyclone at lower latitudes has a tendency to drift poleward and westward more rapidly. But this cannot be explained by beta effect alone because the beta parameter reduces only by 11% from 10–30°N. De Maria (1985) reported that the track of the cyclone is highly dependent on the size change

✉ Hari Prasad Dasari
  hari.dasari@kaust.edu.sa

1 Physical Sciences and Engineering Division, King Abdullah
   University of Science and Technology (KAUST), Thuwal,
   Saudi Arabia

2 Department of Meteorology and Oceanography, Andhra
   University, Visakhaptnam 530003, India

3 Present Address: CPTEC–INPE, Cachoeira Paulista, Brazil

of the vortex and this was confirmed by the study of Fiorino and Elsberry (1989a, b). For the initial symmetric circulation or quasi-steady state in isolated vortices with positive angular momentum, both the beta drift speed and its meridional components are approximately equal to the square root of the total relative angular momentum (Wang and Li 1992). In this study, the total relative angular momentum of the storm is determined with the outer circulation of the vortex and the large circle centered over the vortex. In reality, the tropical cyclones do not maintain perfect symmetry; the asymmetry highly depends on the storm size, intensity, translation speed and direction (Chan and Gray 1982; Chan 1985) of the storm.

The high value of positive relative vortices in vortices advected by the large-scale environmental circulation, called as the steering flow is concentrated within a few kilometers of radius from the center of a tropical cyclone. It is difficult to separate environmental steering flows from tropical cyclone circulations. The steering flow advection depends on the height and radial distance from the tropical cyclone center. The observational study of Franklin (1990) showed that the deep layer (i.e., 1000 to 150/100 hPa) mean steering is correlated better with the storm motion than any other single level steering. The probable reason being that the vertical coupling between boundary layer and the upper-most tropospheric layer is associated with large divergence/convergence inducing vorticity advection (Chan 1984). Holland (1984) suggested that the vertical mean steering between 850 and 300 hPa is the optimum for explaining cyclone movement but failed to explain the movement of strong and weak tropical cyclones. As the cyclone intensifies, it has normally a deeper cyclonic circulation that must be steered by a deeper layer of the environmental flow (Velden and Leslie 1991). Gray (1989) noted that vertically averaged rawinsonde composite winds between 850 and 300 hPa are useful for the storm motion and reported that the steering flow averaged over inner radial bands produced better agreement with the storm motion. Franklin et al. (1996), concluded that the tropical cyclone motion is well correlated with the deep mean flow averaged over 3 degrees of latitude from the center of the inner core region. In this study, the steering flows over the inner core region, including the environmental flow and the secondary steering flow generated by internal dynamics, are important factors for the tropical cyclone motion. Kekuchi and Wang (2010) using 30 years of data found that the substantial number ($\sim 60\%$) of tropical cyclones formed in association with intraseasonal oscillations (ISO). They also found that over 70% of ISO-related genesis is associated with northward propagating boreal summer intraseasonal oscillation (BISO) and up to 30% the east ward propagating Madden–Julion Oscillation (MJO). Evan and Camargo (2011) found that the post-monsoon cyclones formed in either Bay of Bengal or Arabian Sea but not in both during the same year.

In a recent review, Roy and Kavordanyi (2012) discuss several techniques used for forecasting the track of tropical cyclone movement. Some of the techniques mentioned by them are: (1) Persistence forecasting, (2) Climatology forecasting, (3) Integration of the above two, (4) Using synoptic data, (5) Dynamical technique using numerical models and (6) neural network-based techniques. Belangar et al. (2012) made an analysis of predictability of NIO cyclones they use ECMWF variable ensemble prediction system (VAREPS). They found VAREPS provides superior post-genesis track forecast for lead times greater than 12 h compared to other models. Osuri et al. (2013) evaluated the performance of advanced research version of weather research and forecasting model in real time-prediction of tropical cyclones over NIO. The tropical storm HudHud prediction on real time based is attempted by Nadimpalli et al. (2016). Attempts have also been made to assimilate Doppler weather radar observations the Bay of Bengal tropical cyclone prediction (Osuri et al. 2015). Ali et al. (2007) used the neural network technique to predict the track of the NIO cyclones. However, none of these above studies attempted to understand the dynamical process that involved in explaining the westward movement of tropical cyclone.

In the present study, we made an attempt to identify the possible mechanisms for westward movement of the Bay of Bengal cyclone, LEHAR (details are given in Sect. 3). The advanced research weather research and forecasting model (ARW) is used for this study. The model results are divided and discussed in two parts. The first part deals with the model performance on tropical cyclone characteristics. The second part explains the method to infer the westward movement of a tropical cyclone. The complete vorticity equation to diagnose the relative importance of different terms into the tendency of the vorticity near the cyclone center is studied to explain the physical process responsible for the movement of LEHAR. To our knowledge, this method of analysis for the movement of a tropical cyclone has not been used so far.

2 Details of the model and methodology

The ARW model version 3.5.1 (Skamarock et al. 2008), a primitive equation, non-hydrostatic model with the terrain following coordinate system, developed by NCEP/NCAR, USA is used in the present study. The ARW model is configured with two domains (Fig. 1) of horizontal resolutions of 27 and 9 km with 35 vertical levels. The used physics options for this study are KF2 (Kain 2004) for cumulus convection, WSM3 explicit microphysics, Dudhia scheme (Dudhia 1989) for shortwave radiation processes, RRTM scheme for longwave radiation processes (Mlawer

Fig. 1 Model domains (27 and 9 km)

et al. 1997), the Yonsei University scheme for the PBL turbulence (Hong et al. 2006; Nolan et al 2009a, 2009b) and five layer soil thermal diffusion scheme for land surface processes. As the main objective of the study is to explain the westward movement of the storm, we used the grid resolution, size of the domains, and the physics options chosen for this study are same as the previous studies (Sathi Devi et al. 2006; Bhaskar Rao and Hari Prasad 2006a, b; Srinivas et al. 2007, 2013; Bhaskarrao et al. 2009, 2010; Hari Prasad and Bhaskar rao 2015) to maintain the consistency with the previous studies.

The GFS model forecasting fields available at $0.5° \times 0.5°$ horizontal resolution are used for initial conditions and boundary conditions are updated at every 3 h interval. The model is integrated for 5 days starting from 0000 UTC of 24 November 2013. The model products are compared with the India Meteorological Department Observations (2014) and Satellite products (KALPANA, CIMSS-Cooperative Institute for Meteorological Satellite Studies).

2.1 Tendency of relative vorticity analysis

For obtaining the tendency of relative vorticity, we used the following equation

$$\underbrace{\frac{\partial \xi_r}{\partial t}}_{A} = \underbrace{-u\frac{\partial \xi_r}{\partial x} - v\frac{\partial \xi_r}{\partial y}}_{B} \underbrace{- \omega\frac{\partial \xi_r}{\partial p}}_{C} \underbrace{- v\frac{\partial f_r}{\partial y}}_{D} \underbrace{+ f_c\frac{\partial \omega}{\partial p}}_{E} \underbrace{+ \xi_r\frac{\partial \omega}{\partial p}}_{F} \underbrace{+ \frac{\partial u}{\partial p}\cdot\frac{\partial \omega}{\partial y} - \frac{\partial v}{\partial p}\cdot\frac{\partial \omega}{\partial x}}_{G}$$

(1)

Different terms of Eq. 1 have the following interpretation. Where u, v and ω are zonal, meridional and vertical wind components, respectively, ξ_r is the relative vorticity and f_c is the Coriolis parameter.

The term A is called the tendency of vorticity (TOTAL). The term B is the horizontal advection (HADV) is the zonal and meridional advection of the relative vorticity and the term C is the vertical advection (VADV). Term D is the beta effect representing the advection of planetary vorticity (BETA). The terms E and F are the stretching terms (STR1 and STR2).

For tropical cyclones, the coriolis force (f) is small and the stretching term associated with vorticity is higher. When the raising motion increases with height, the vortex tube stretches and to maintain the mass balance, the radius decreases which inturn increases the spin or vorticity. The two stretching terms account for earth's rotation and relative vorticity. And the term G (TILT) is the tilting term or solenoid term and its contribution for the vorticity can be interpreted as follows (Hess 1959). The first term $(\frac{\partial v}{\partial p}\cdot\frac{\partial \omega}{\partial x})$ indicates that when the raising motion increases in the x-direction and the changes in meridional wind increases with height because of –ve sign its contribution towards +ve vorticity tendency i.e., the relative vorticity increases with time. This vertical shear constitutes a vorticity about the horizontal in the east–west axis. A similar interpretation can be given to second term but the vertical shear constitutes in the north–south axis. The various terms A to G of the vorticity tendency equation are computed at every 1 h interval starting from 0000 UTC of 24 November 2013. At the stipulated time (t), the center of the storm is identified and then the storm center is divided into four sectors (North East-NE, North West-NW, South West-SW and South East-SE). In each sector at around 55 km, radius the relative vorticity field is examined to identify the location of the maximum relative vorticity tendency. At these four grid locations, all terms of the vorticity tendency equation are computed at (t-1) hours to identify the contributions from various terms on the right hand side of the Eq. (1). This means that the vorticity change at the identified grid location at time t is the resultant of the contributions of all different terms at the same grid location at time (t-1). It is assumed that the vortex will move to the nearest positive vorticity tendency. Though it may be desirable to have smaller time lag (Δt), the time lag of 1 h has been chosen to have a smooth distribution of the vorticity tendency and the contributing terms.

To diagnose convection and strong ascending motion, we use lightning data. Daily lightening data for tropical cyclone LEHAR are retrieved from the lightning imaging sensor (LIS) of tropical rainfall measuring mission (TRMM) satellite products LIS/OTD at 2.5° grid low-

resolution time series (LRTS, version 2.3) datasets (https://ghrc.msfc.nasa.gov) are used.

3 Description of LEHAR cyclone

A depression formed over Bay of Bengal (BOB) on 23 November 2013 and intensified into a cyclonic storm named LEHAR with center at 10.0°N/95.0°E by the morning of 24 November. It moved in northwest direction and intensified as a severe cyclonic storm (18 m s^{-1}) in 24 h. It emerged into southeast BOB and moved west-northwestward, later intensified into a very severe cyclonic storm by 2100 UTC 26 November. LEHAR attained the maximum intensity of 75 knots at 1800 UTC of 26 and the same intensity continued till 0300 UTC of 27 November. After that, the system moved west-northwestwards over west central BOB and it rapidly started weakening from afternoon of 27 November. It further weakened into a cyclonic storm at 1800 UTC of 27 November 2013 with center near 15.0° N/84.0° E over west-central BOB.

LEHAR is chosen for this study because it is having nearly 5 days of life period and further it moved north-westward first, then a little northeast direction and later that it completely moved west-northwest direction. Thus, to explain the westward movement of the cyclone using vorticity tendency equation, LEHAR is a good example.

4 Results and discussions

The numerical model results from thes 9 km domain are analysed and discussed to verify how well the model simulates the features of LEHAR and then the contribution of different terms of the vorticity equation, thereby elucidating the physical mechanisms responsible for the westward movement of LEHAR.

4.1 Sea level pressure and winds

The time series of central sea level pressure (CSLP) and maximum wind (MW) for the model and observations of IMD, JTWC (Japan Typhoon Warning Center) and RAMMB (Regional and Meso-scale Meteorological Branch, NOAA/NESDIS/STAR/RAMMB and CIRA) satellite derived winds at 25 km resolution are presented and discussed (Fig. 2a and 2b). The model results of CSLP show (Fig. 2a) that they agree well with the JTWC and RAMMB compared to IMD observations. The model is able to produce a steady intensification and reached minimum CSLP of 967 hPa at 0000 UTC of 26 November, sustained for a period of about 6–12 h, and then dissipated in agreement with the JTWC and RAMMB. But the IMD observations do not show the maximum intensity and do not coincide with any other observations. The correlation values of pressure drop between model and IMD is 0.43, JTWC is 0.75 and RABBM is 0.57 significant at 95% or more by Student's t test. The probable reason for these higher errors with IMD is may be due to the methodology that adopted for identification of the storm intensity. The IMD is defining the storm CSLP and MW qualitatively based on Satellite imagery, where as the JTWC and RABBM are using some mathematical algorithm in defining the storm strength. Similar features are seen in maximum winds in Fig. 2b. The model-produced maximum winds show increasing and decreasing values with the higher magnitude as compared to all observations. The observations show more smooth values than the model, this may be due to fact that the model generates more asymmetries over cyclone core region due to its higher resolution of 9 km. The radius of maximum winds is the distance between the center of a cyclone and its band of strongest winds, from model and RAMMB (Fig. 2c) it indicates that the radius of maximum wind (RMW) of the storm at mature stage is located around 20 km radius and it remains for a 36-h period during intensification and mature stage of the storm in good agreement with the RABBM.

4.2 Divergence analysis

The divergence fields at 850 and 200 hPa from model are computed and analyzed. The analysis at 850 hPa shows (Fig. 3) that from 0000 UTC of 26 to 0600 UTC of 27 October, a strong narrow low-level convergence (shaded region) of about -200×10^{-5} s^{-1} around the cyclonic storm is noticed and a weaker divergence (contours) of about 25×10^{-5} s^{-1} is also seen. The magnitudes of the convergence regions are ten times more than the divergence and the region of convergence is very small and narrow as compared to the regions associated with the divergence. These patterns clearly indicate that the storm is highly concentrated at narrow region and expected strong vertical uplift of the moisture, associated convection and severe rainfall over the storm regions.

Similarly at 200 hPa, a wider area of divergence flow (contours) of about 50×10^{-5} s^{-1} is noted (Fig. 4) and this feature existed throughout the period of cyclone intensification. The center of low-level convergence is not exactly at the same place at the higher level. It is tilted towards west after 0000 UTC of 27 November and is due to the cyclone nearing to the coast, it starts weakening and the strength of the storm at lower level reduces due to the friction on inward or converging flow. In addition to explaining the features of the upper-level divergence and extension of convergence, the model-predicted convergence at 250 hPa (Fig. 5a, shaded +ve values) along with
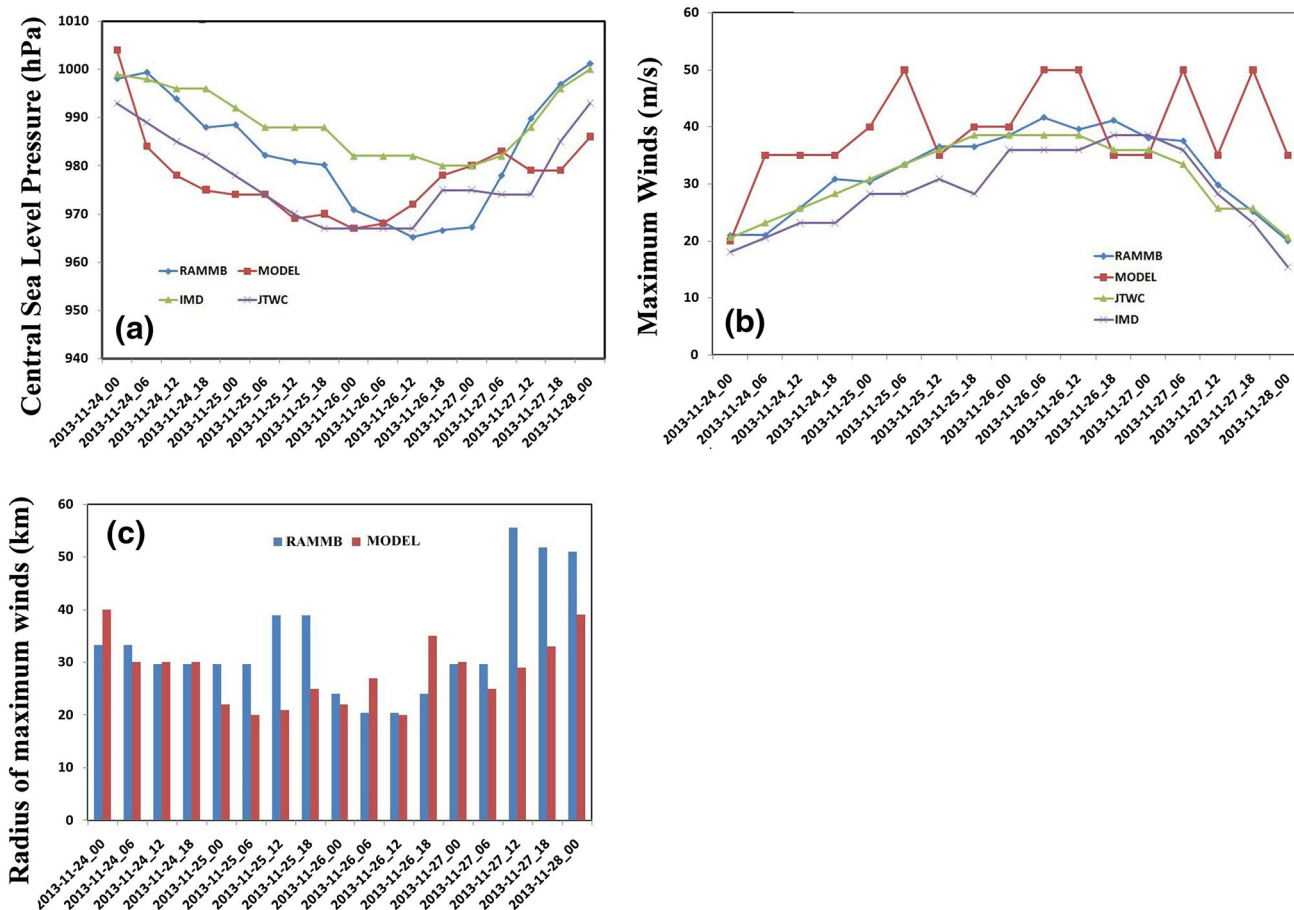
Fig. 2 Time series of **a** central sea level pressure (hPa). **b** Maximum wind (m/sec). **c** Radius of maximum wind (Km)

the CIMSS (Cooperative Institute for Meteorological Satellite)-derived convergence (Fig. 5b) region (–ve contours) are plotted and discussed. A wider area of divergence at higher levels and a narrow region of convergence around the cyclonic storm are well predicted by the model as can be seen in satellite fields. The difference in the divergence from 150 to 300 hPa shows (Fig. 5c and 5d) over a wide area of convergence zone with completely outward flow extended up to 300 hPa. The convergence over north side and divergence over south side of the storm are well predicted by the model as seen in satellite fields. From the above analysis, we infer that to conserve the mass, a strong rising motion near the center over a small area should be replaced by sinking motion over a wide area at upper levels.

4.3 Cyclone characteristics

The analysis of cyclone cloud characteristics at mature stage of the storm is presented (Fig. 6) and discussed. The model-predicted cloud cover shows that the concentrated convective clouds around the eye region, wide region of

cloud bands at the periphery of the eye and eye-wall regions are well agreed with the KALPANA-1 VHRR Satellite imagery.

The height section analysis for different variables along the eye of the storm (13.42°N) at mature stage 0300 UTC 26 November 2013 is presented in Fig. 7. The maximum winds (Fig. 7a) of around 56 m s^{-1} at eye-wall region around 50–70 km from the center of the storm extended up to 300 hPa in east side and up to 500 hPa in west of the storm are noticed. The cyclone winds of > 26 m s^{-1} are seen around 500 km from the center of the storm on both east and west directions suggest that the size of storm at the mature stage is of about 1000 km. A clam region with a diameter of about 50 km in the eye region is found. The upward motions (Fig. 7b) along with the higher radar reflectivity (Fig. 7c) are very clearly seen around the eye-wall regions on west side of the storm and downward motions on the east side of the storm. This makes vorticity to increase to west of the storm significantly which forces storm to move westward.

The high values with a wide area on the west side are an indication that the clouds associated on the west side are
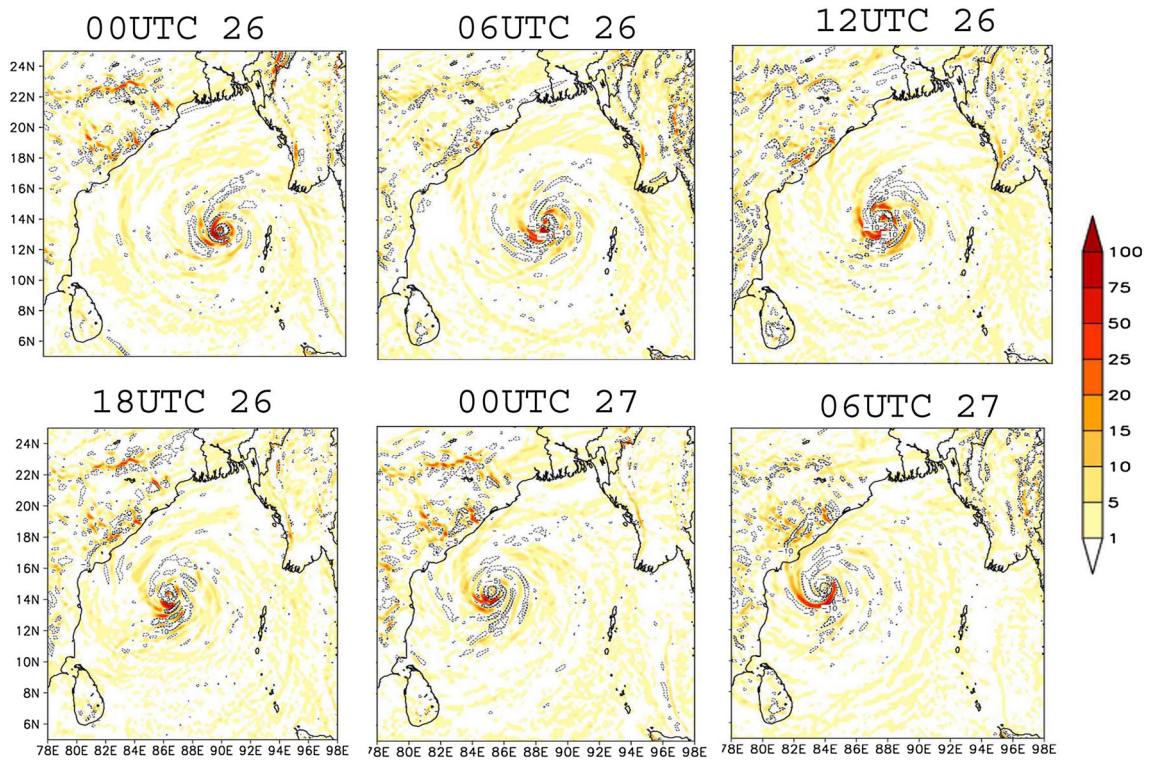
Fig. 3 Divergence (1e–5) at 850 hPa for different times (convergence is shaded and divergence is in contours)
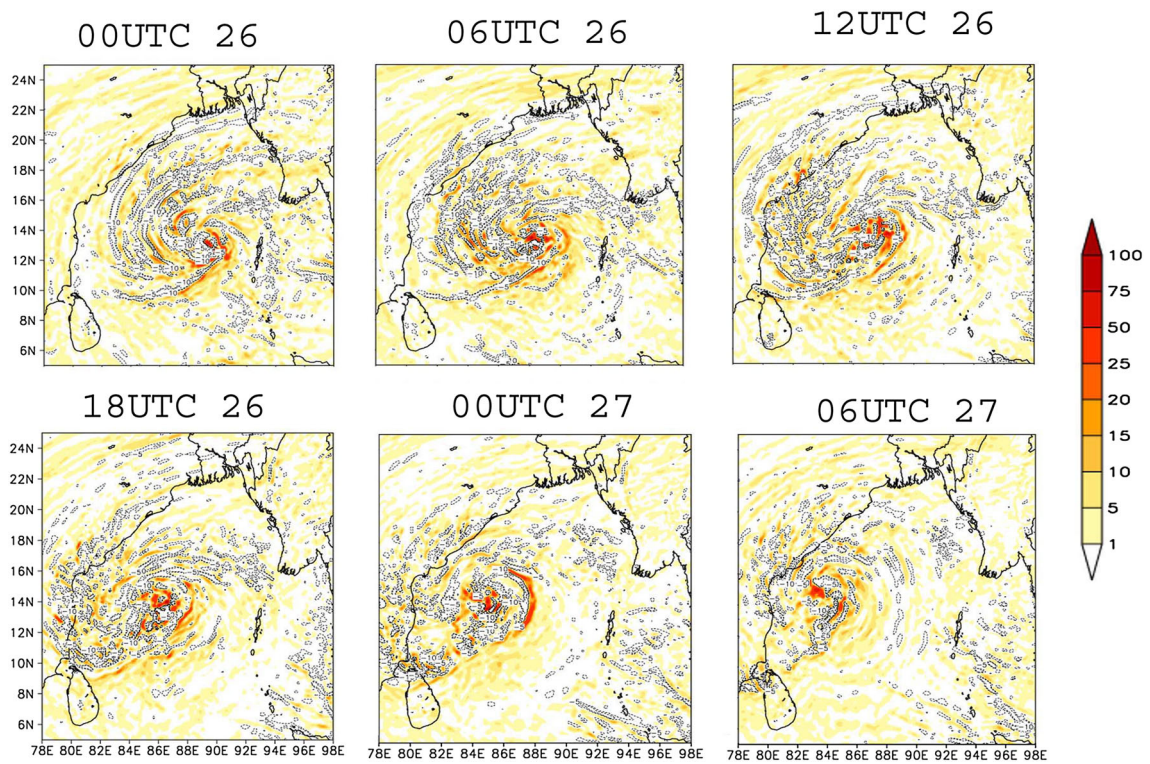

Fig. 4 Divergence (1e–5) at 200 hPa for different times (convergence is shaded and divergence is in contours)
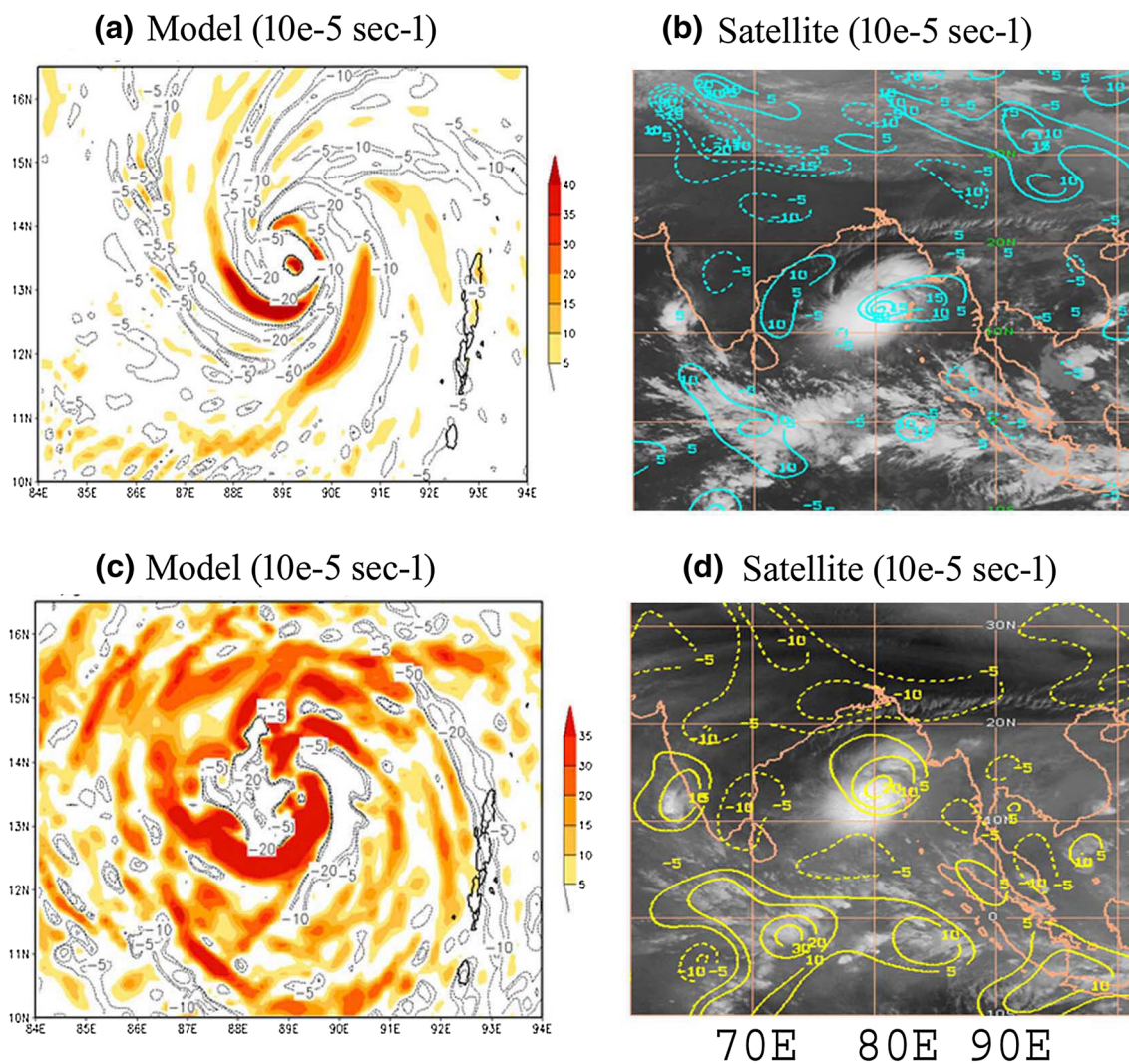
(a) Model (10e-5 sec-1)

(b) Satellite (10e-5 sec-1)

(c) Model (10e-5 sec-1)

(d) Satellite (10e-5 sec-1)

Fig. 5 Convergence regions at 200 hPa (top panel) and divergence (bottom panel, 150–300 hPa) for model and CIMSS satellite products at mature stage (on 0300 UTC 26 November 2013) of the cyclone

with the highest vertical velocity. This shows that the storm is likely to move still in a westward direction from its current position. Although at this stage the westward movement explained qualitatively, at a later stage we explained more accurately with the quantitative analysis. The increase of the temperature after 12 h (Fig. 7d) shows that the warm core region (about 9 °C increase) at the center of the storm is increasing and extended up to 400 hPa level. The results also show a slight tilt towards west with a conical shape, smaller area at the surface and wider area at the upper levels, of the higher temperatures and indicates that the warm core region leads to an increase of latent heat release at mid to upper levels and further leads to high amount of clouds. Therefore, the latent heat provides the energy that increases vertical circulation and mainly the strength of the storm.

Figure 8 illustrates the distribution of lightning flash rates during the period 25–28 November 2013 in the four sectors, northeast (NE), southeast (SE), southwest (SW) and northwest (NW). The figure shows the flash rates are higher in the SW and NW sectors of the cyclone Lehar. Earlier studies (Leary and Ritchies 2009) have shown that lightening can be used as a proxy of intense deep convective clouds because only intense deep clouds will have necessary fundamental conditions, strong vertical updraft and super cooled water. Super cooled water is considered as the basic component for cloud electrification. Super cooled water after freeze onto the graupel becomes heavy and fall through the cloud. The following graupel particles collide with the lighter ice particles during which positive charge is transferred to the ice particles. Strong updraft will weep the positive ice particles higher onto the cloud
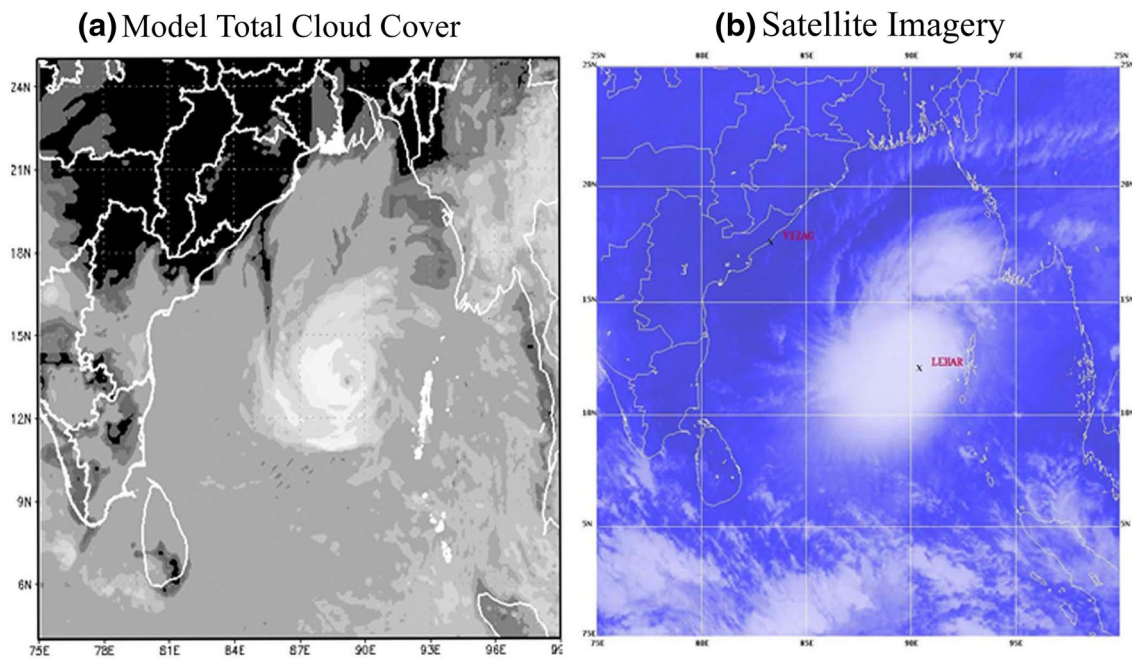
Fig. 6 Total cloud-cover **a** model and **b** satellite (Kalpana) at mature stage (on 0300 UTC 26 November 2013) of the cyclone
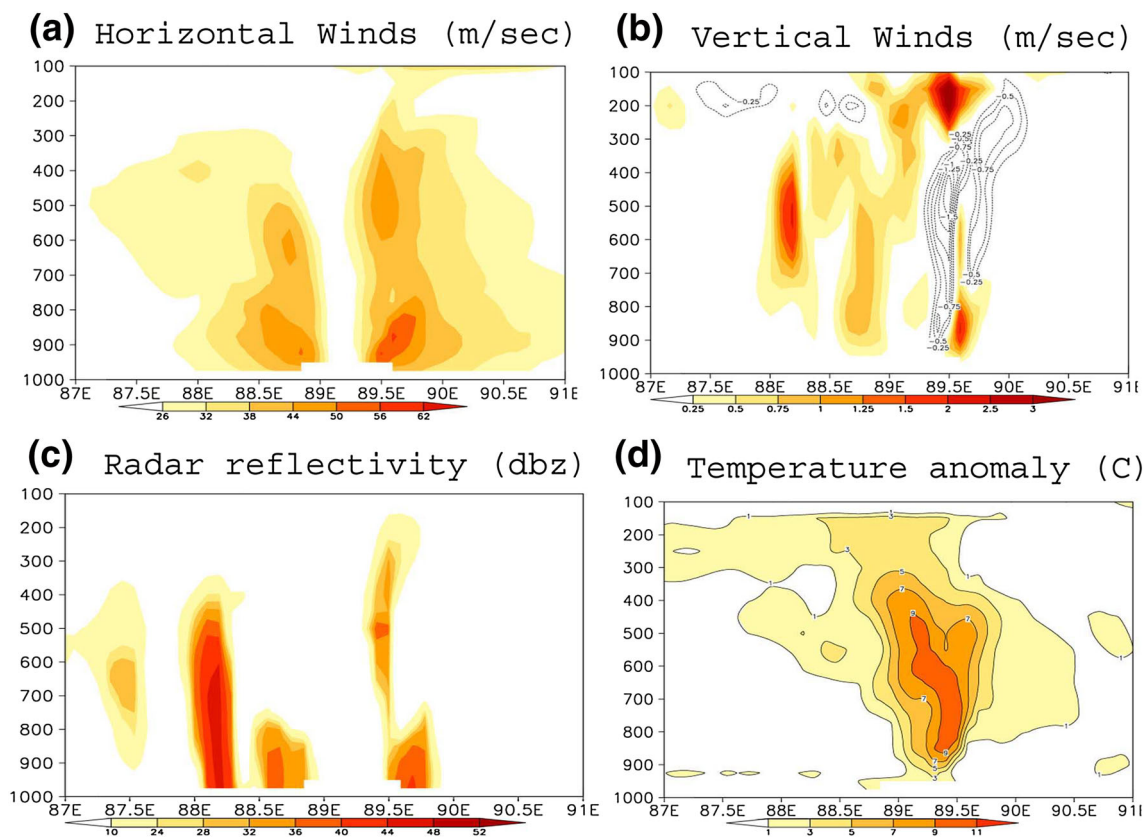

Fig. 7 Height section of different parameters along latitude 13.4 N at mature stage of the cyclone

leaving the heavier negative graupel particles below resulting dipole charge distribution within the cloud. Takahashi ([1978](#)) established that highest electrification occurs when the smallest ice crystals present in the lowest temperatures of the cloud. Electric discharge occurs when the separation between the charges is large enough. High

Fig. 8 Distribution of mean lightning flash rates in tropical cyclone LEHAR during the period 25–28 November 2013 in the four sectors, northeast (NE), southeast (SE), southwest (SW) and northwest (NW)
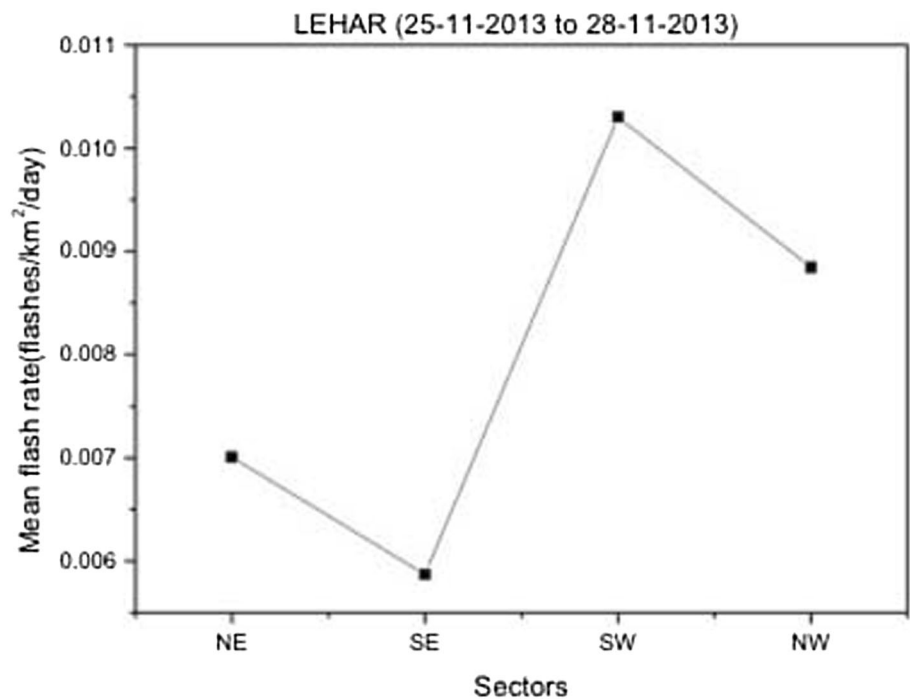

flash rates clearly indicate deep convection associated strong vertical velocities in NW and SW sectors. Later, we show with vorticity analysis that the storm is likely to move in the westward direction as a result of high vorticity tendency in the SW and NW sectors.

The model-predicted spatial distribution of rainfall shows (Fig. 9) that a wide area of storm region is with heavy rainfall of 40 cm in a day with the maxima over southwest of the storm. The spatial distribution of the model produced rainfall pattern and its intensity is well agreeing with the tropical rainfall measuring mission (TRMM) 3B42 version 7 data (Huffman et al. 2007, Huffman and Bolvin 2012).

4.4 Vorticity analysis

Even though the objective of the study is to explain the westward propagation of the LEHAR, in the previous section, an extensive analysis is made to verify the model performance on different cyclone features. The model is able to predict several characteristics of the cyclone. In this section, the influence of different physical processes associated with the vorticity for the westward movement is explained. For this analysis, we used the level 850 hPa as a reference level to compute all terms involved in vorticity tendency equation. The reason is that at this level the relative vorticity at mature stage is with the maximum value of 330×10^{-5} s^{-1} (Fig. 10).

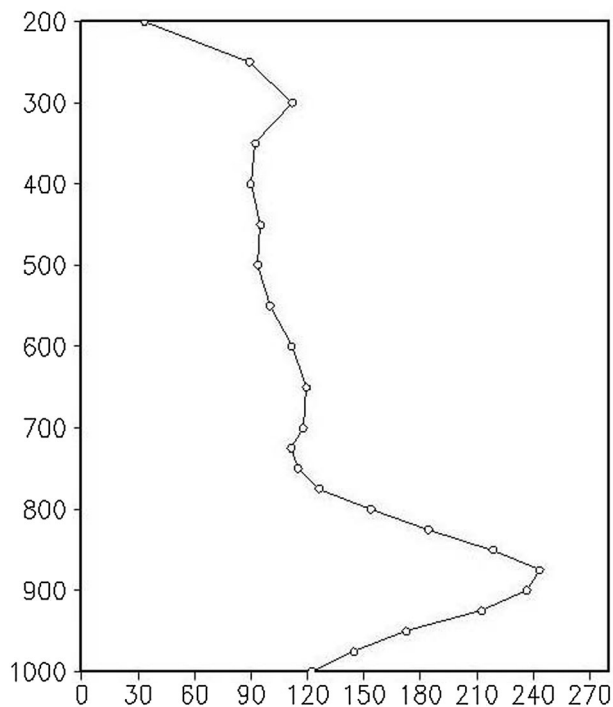**Fig. 9** Daily accumulated rainfall (mm/day) **a** Model and **b** TRMM
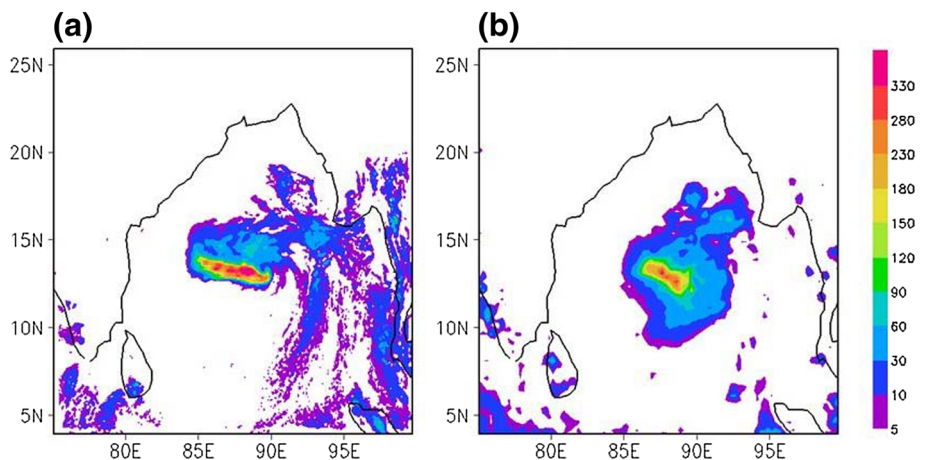
Fig. 10 Vertical profile of vorticity ($\times 10^{-5}$ s^{-1}) at the location of maximum vorticity during mature stage of the LEHAR

To delineate the physical process responsible for the westward movement of the storm, a diagnostic analysis of vorticity equation is made. The storm core region from the center is divided into four sectors, namely northeast (NE), northwest (NW), southwest (SW) and southeast (SE) at every hour interval of the model simulation period starting from initial time of integration. In each sector, a point around 50 km radius is identified from the center and computed every term of vorticity equation. All the required variables at every hour interval are extracted for three levels and vorticity tendency is computed from Eq. 1 and presented (Fig. 11). The results indicate that the vorticity tendency at southwest sector is much higher than any other sector (please see the scale of ordinate). It steadily increased to nearly 1450×10^{-8} s^{-1} around 1200 UTC of 25 and then slowly starts reducing its intensity. Throughout the duration of the cyclone, the maximum vorticity is seen in the southwest sector, which is contributed mainly by the SRT2. Along with the southwest sector, the northwest sector also shows higher value of its intensity up to 1200 UTC of 25 and then decreased. In this too, the STR2 term contributed more than any other term to maximum value of the positive vorticity tendency. But two maxima in two directions of northwest and southwest directions lead to a resultant or intermediate path of westward movement. During westward migration, time around 0000 UTC of 25 November, the HADV term in northwest sector completely changes its direction with increased intensity. This can be

due to the flow in a northwest moving cyclone at NW is easterly flow and in this sector the winds are trying to change their directions. This causes stronger westward movement instead of northwest movement and so the tendency becomes negative over this sector and vortex weakens. The track of the LEHAR obtained from different sources (Fig. 12) shows that the track from vorticity tendency is in a good agreement amongst all shows that the feasibility of using the present method for the tropical cyclone track prediction.

4.5 CISK or WISH?

Charney and Eliassen (1964) proposed the conditional instability of second kind (CISK), a cooperative interaction between a cumulus scale and the large-scale disturbance, since the linear instability leads only to cumulus scale disturbance for the cyclone developed. In this theory, a small amplitude disturbance superimposed on background flow is tested for instability and they proposed that the instability of this disturbance leads to amplification and finally to a mature cyclone. Although this theory successfully explained the development of the extratropical cyclones there is a little evidence that this type of instability leads to observed scales of tropical cyclones?

Recently, a new theory has been proposed by Emmanuel (2004) named as wind-induced surface heat exchange (WISH). In this theory, the role of underlined sea surface is stressed. An initial disturbance provided winds at the surface and this increases the evaporation from sea leading to saturation. Emmanuel (2004) shows that most of the entropy increases near the eye wall due to the strong equivalent potential temperature gradient. Thus, in this theory the purpose of cumulus convection is not to provide an internal heat source but to produce a moist adiabatic lapse rate.

To verify the functioning of the WISH in LEHAR cyclone, the equivalent potential temperature at different stages of before (0300 UTC 25), during (0300 UTC 26) and after (0300 UTC 27) the mature stage are plotted (Fig. 13) and analyzed. The model predicted the strong gradients in equivalent potential temperatures near the eye region and the results confirm that the role of WISH in development of LEHAR.

5 Summary

In the present paper, a diagnostic analysis is made to infer the westward movement of the tropical cyclone that formed over Bay of Bengal named LEHAR 23 November 2013. The ARW model with two-way interactive nested domains of 27 and 9 km horizontal and 35 vertical levels are used for this study.
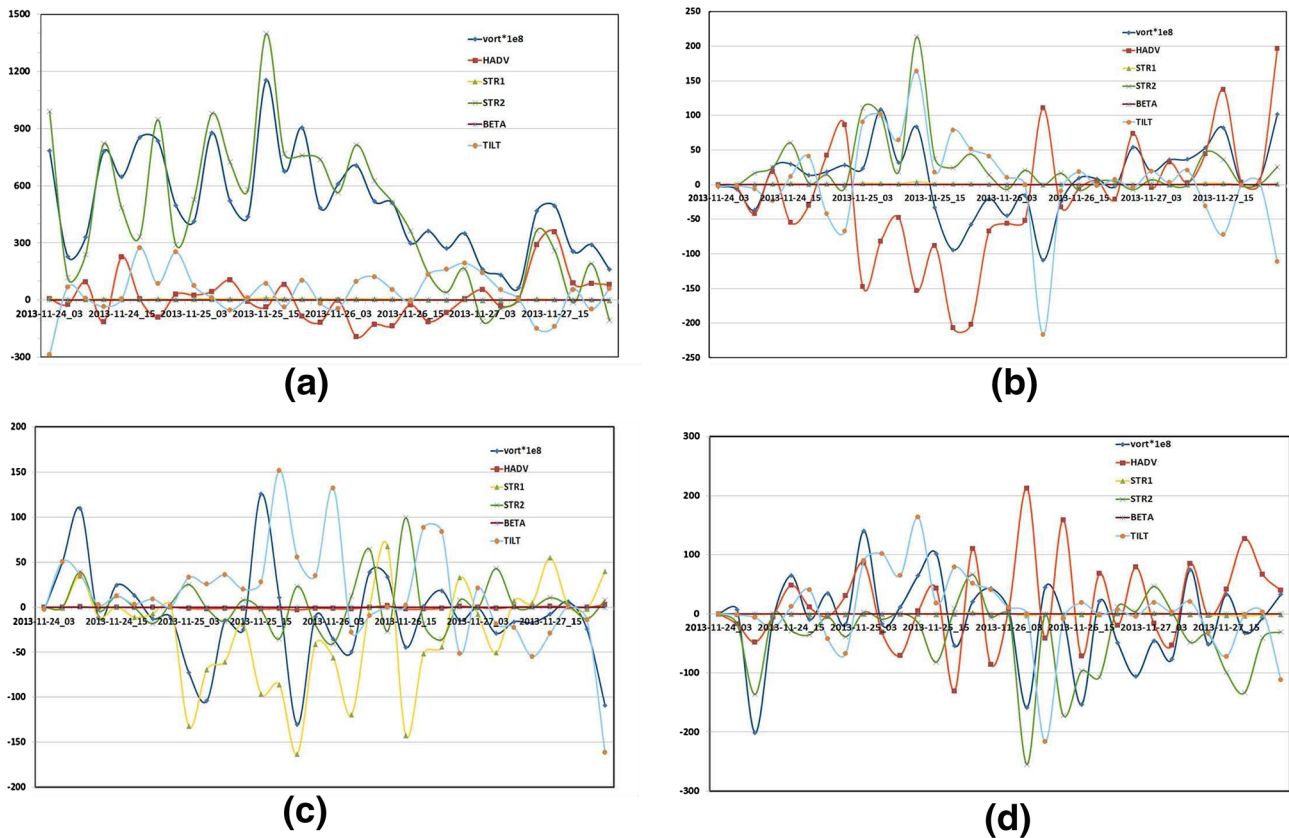
(a)

(b)

(c)

(d)

Fig. 11 Vorticity tendency and its associated terms in four **a** southwest **b** northwest **c** northeast and **d** southeast sectors of the cyclone storm
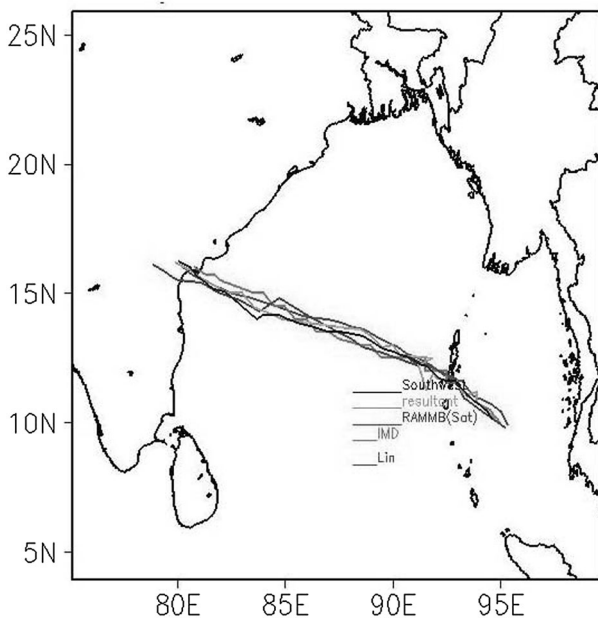

Fig. 12 Model-predicted track along with the observations of IMD, JTWC and RAMMB

The model results are analyzed with a view to verify the performance of the model in the simulating LEHAR. The model-predicted CSLP shows the minimum of around 967 hPa at 0300 UTC of 26 November, the satellite measured CSLP is 965 hPa but at a later time of 0900 UTC of 26 November. The JTWC observations coincide well with the model results, while the IMD observations show a much weaker vortex of CSLP 980 hPa. The MW in the model is a little higher than in the observations. The predicted RMW at different times agrees well with the observations at beginning but later seem to underestimate. The model divergence analysis at 850 and 200 hPa shows that the strong convergence near the center of the vortex with intense vertical motion is compensated by divergence and slow descent over a large region at higher levels, thus conserving the mass. The vorticity measured with satellite winds at different levels shows a vertical tilt towards the west with height. The model-inferred temperature tendency also shows that the maximum temperature tilts westwards. The rising motion and higher radar reflectivity are on the west side of the vortex. These results confirmed that the model-predicted values are well agreed with the observed aspects of LEHAR. The lightening flash rates in all four sectors of the storm are analyzed and the highest flash rates in SW and NW sectors are clearly noticed. This infers the deep convection associated with high vertical velocities in these two sectors.
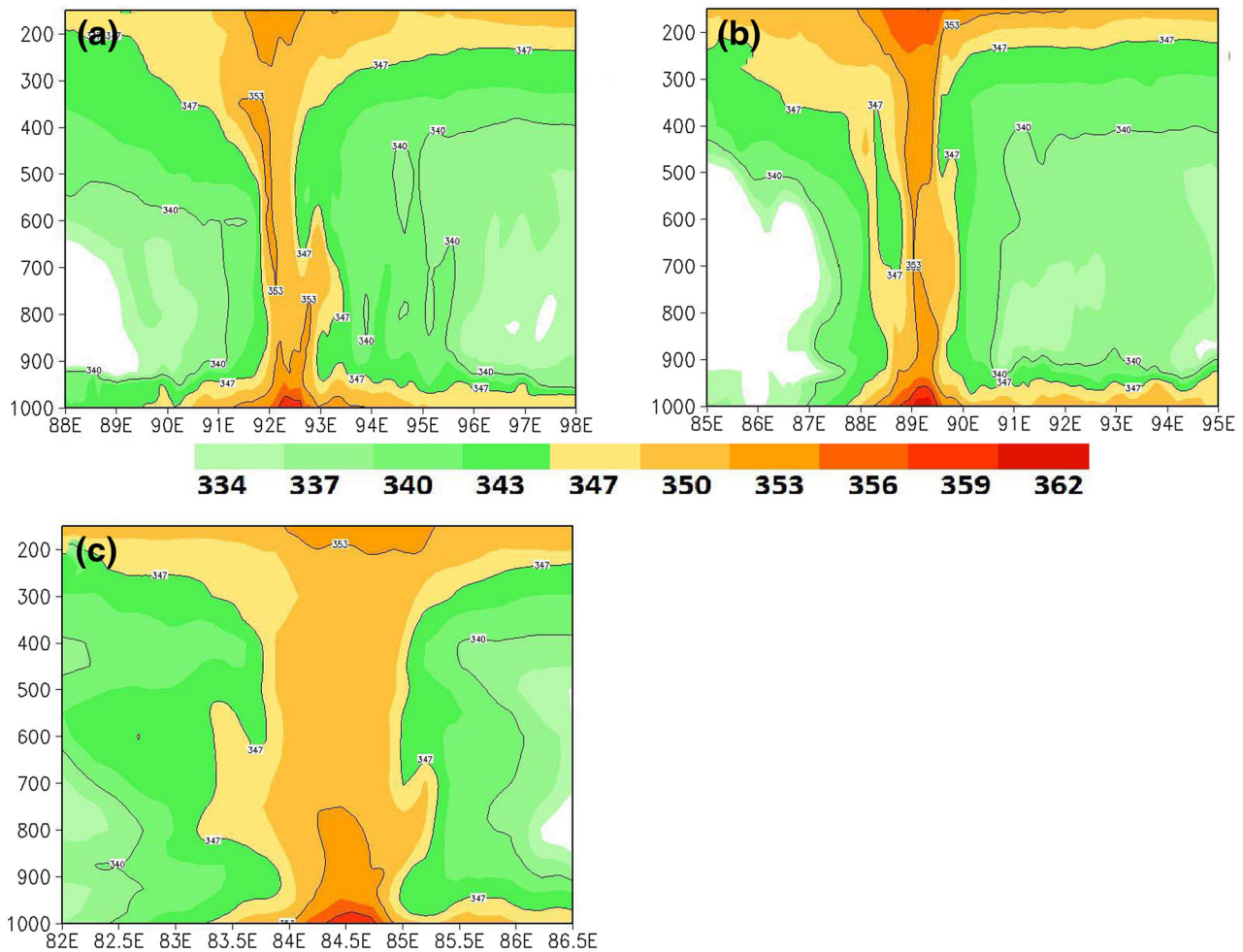
Fig. 13 Longitudinal-height section of equivalent potential temperature (K) at 0300 UTC of **a** 25 **b** 26 and **c** 27 November 2013

To infer the sector of the maximum vorticity changes at different times, each term of the complete vorticity equation in four sectors NW, NE, SW and SE are computed and analysed. At every sector, a point at around 50 km radius from the vortex center is identified and all terms are in the tendency equation. It is assumed that the vortex moves in the direction of the +ve vorticity change at the nearest point from the center. This analysis shows that the STR2 is highest and located in the SW sector. There is secondary maximum in the NW sector. Thus, vortex moves along the resultant of the two regions of NW and SW, i.e., the vortex moves westwards. The STR2 makes the vortex stretch in the vertical. This increases the vertical extension to keep the mass balance makes the radius decrease. This decrease of the radius inturn makes the spin to increase thus increases the vorticity. Since the STR2 is the highest in NW and SW sectors, the resultant makes vortex move westwards. To the best of our knowledge, the methods suggested here has not been used earlier to diagnose tropical cyclone movement. However, the diagnostics at a point may not be appropriate but this method should be adopted for the area- or volume-integrated (averaged) values. Some caution should be exercised to apply this method directly (Haynes and McIntyre, 1987).

References

Adem (1956) A series solution for the barotropic vorticity equation and its application in the study of atmospheric vortices. Tellus 8:364–372

Ali MM, Jagadeesh PSV, Jain S (2007) Effects of eddies and dynamic topography on the Bay of Bengal cyclone intensity. Eos, Transactions, Am Geophysical Union 88:93–95

Belangar JI, Webster PJ, Curry JA, Jelinik MT (2012) Extended prediction of north Indian ocean Tropical cyclones. Wea. Froecasting 27:757–769

BhaskarRao DV, Hari Prasad D (2006a) Sensitivity of tropical cyclone intensification to boundary layer and convective processes. Nat Hazards. https://doi.org/10.1007/s11069-006-9052-7

BhaskarRao DV, Hari Prasad D (2006b) Numerical prediction of the Orissa super cyclone (1999): sensitivity to the parameterisation of convection, boundary layer and explicit moisture processes. Mausam 57:61–78

BhaskarRao DV, Hari Prasad D, Srinivas D (2009) Impact of horizontal resolution and the advantages of the nested domains approach in the prediction of tropical cyclone intensification and movement. J Geophysical Res (Atmosphere) 114:D11106. https://doi.org/10.1029/2008JD011623

BhaskarRao DV, Hari Prasad D, Srinivas D, Anjaneyulu Y (2010) Role of vertical resolution in numerical models towards the intensification, structure and track of tropical cyclones. Mar Geodesy 33(4):338–355. https://doi.org/10.1080/01490419.2010.518066

Chan JCL (1984) Definition of the steering flow for tropical cyclone motion. In: Proc. 15th Conf. Hurr. Trop. Meteor. Soc., Boston MA, vol. 02108, pp 559-566

Chan JC-L (1985) Identification of the steering flow for tropical cyclone motion from objectively analysed wind fields. Mon Wea Rev 113:106–116

Chan JC-L, Gray WM (1982) Tropical cyclone movement and surrounding flow relationships. Mon Wea Rev 110:1354–1374

Chan JC-L, Williams RT (1987) Analytical and numerical studies of the beta-effect in tropical cyclone motion. Part 1: zero mean flow. J Atmos Sci 44:1257–1265

Charney JG, Eliassen A (1964) On the growth of hurricane depression. J Atmos Sci 21:68–75

DeMaria M (1985) Tropical cyclone motion in a non-divergent barotropic model. Mon Wea Rev 113:1199–1209

Dudhia J (1989) Numerical study of convection observed during winter monsoon experiment using a mesoscale two-dimensional model. J Atmos Sci 46:3077–3107

Emanuel K (2004) Tropical cyclone energetics and structure. In: Fedorovich E, Rotunno R, Stevens B (eds) Atmospheric turbulence and mesoscale meteorology. Cambridge Univ. Press, Cambridge, pp 165–191

Evan Amato T, Camargo Suzana J (2011) A Climatology of Arabian Sea Cyclonic Storms. J. Climate 24:140–158

Fiorino M, Elsberry RL (1989a) Some aspects of vortex structure related to tropical cyclone motion. J Atmos Sci 46:975–990

Fiorino M, Elsberry RL (1989b) Contributions to tropical cyclone motion by small, medium and large scales in the initial vortex. Mon Wea Rev 117:721–727

Franklin JL (1990) Drop windsonde observations of the environmental flow of hurricane Josephine (1984), relationships to vortex motion. Mon Wea Rev 118:2732–2744

Franklin JL, Feuer SE, Kaplan J, Aberson SD (1996) Tropical cyclone motion and surrounding flow relationship: searching for beta gyres in omega dropwindsonde datasets. Mon Wea Rev 124:64–84

Gray WM (1989) Summary of ONR sponsored tropical cyclone motion research and future plans, Appendix D of Tech. Rep. NPS 63-89-002, vol 93943. Naval Postgraduate School, Montery, pp 68–79

Hari Prasad D, Bhaskar rao DV (2015) A diagnostic study of Bay of Bengal tropical cyclone (Orissa super cyclone) movement and intensity. Int J Earth Atmos Sc 1(3):115–131

Haynes PH, Mcintyre ME (1987) On the evolution of vorticity and potential vorticity in the presence of diabatic heating and frictional or other forces. J Atmos Sci 44(5):828–841

Hess SL (1959) Introduction to theoretical meteorology. Q J R Meteorol Soc 86(368). doi:10.1002/qj.49708636824

Holland GJ (1984) Tropical cyclone motion: a comparison of theory and observation. J Atmos Sci 41:68–75

Hong S-Y, Noh Y, Dudhia J (2006) A new vertical diffusion package with explicit treatment of entrainment processes. Mon Wea Rev 134:2318–2341

Huffman GJ, Bolvin DT (2012) TRMM and other data precipitation data set documentation. (ftp://meso-a.gsfc.nasa.gov/pub/trmmdocs/3B42_3B43_doc.pdf)

Huffman GJ, Adler RF, Bolvin DT, Gu G, Nelkin EJ, Bowman KP, Hong Y, Stocker EF, Wolff DB (2007) The TRMM multi-satellite precipitation analysis: quasi-global, multi-year, combined-sensor precipitation estimates at fine scale. J Hydro meteorol 8:38–55. https://doi.org/10.1175/JHM560.1

India Meteorological Department (2014) Nwp report on cyclonic storms over the North Indian ocean during 2013. India Meteorological Department. https://202.54.31.51/bias/NWP-CYCLONE-REPORT-2013.pdf

Kain JS (2004) The Kain-Fritsch convective parameterization: an update. J Appl Meteorol 43:170–181

Kikuchi K, Wang B (2010) Formation of tropical cyclones in the northern Indian Ocean associated with two types of tropical intraseasonal oscillation modes. J Meteor Soc Jpn 88:475–496

Krishna KO, Mohanty UC, Routray A, Mohapatra M, Niyogi D (2015a) Real-time track prediction of tropical cyclones over the North Indian Ocean using ARW model. J Appl. Meteor. Climatol 52:2476–2492

Krishna KO, Mohanty UC, Routray A, Mohapatra M, Niyogi D (2015b) Improved prediction of Bay of Bengal tropical cyclones through assimilation of Doppler weather radar observations. Mon Wea Rev 143(11):150501120113009

Leary LA, Ritchies EA (2009) Lightning flash rates as an indicator of tropical cyclones genesis in the Eastern North Pacific. Mon Wea Rev 137:3456–3470

Mlawer EJ, Taubman SJ, Brown PD, Lacono MJ, Clough SA (1997) Radiative transfer for inhomogeneous atmosphere: RRTM, a validated correlated-k model for the long-wave. J Geophys Res 102(D14):16663–16682

Nadimpall Raghu, Osuri Krishna K, Sujata Pattanayak UC, Mohanty MM Nageswararao, Kiran Prasad S (2016) Real-time prediction of movement, intensity and storm surge of very severe cyclonic storm Hudhud over Bay of Bengal using high- resolution dynamical model. Nat Hazards. https://doi.org/10.1007/s11069-016-2155-x

Nolan DS, Zhang JA, Stern DP (2009a) Evaluation of planetary boundary layer parameterizations in tropical cyclones by comparison of in situ observations and high-resolution simulations of hurricane Isabel (2003). Part I: initialization, maximum winds, and the outer-core boundary layer. Mon Wea Rev 137:3651–3674

Nolan DS, Stern DP, Zhang JA (2009b) Evaluation of planetary boundary layer parameterizations in tropical cyclones by comparison of in situ observations and high-resolution simulations of hurricane Isabel (2003). Part II: inner-core boundary layer and eye-wall structure. Mon Wea Rev 137:3675–3698

Rossby (1948) On displacement and intensity changes of atmospheric vortices. J Mar Res 7:175–196

Roy C, Kavordanyi R (2012) Tropical cyclone track forecasting techniques—a review. Atmos Res 104–105:40–69

Sathi Devi K, Hari Prasad D, Bhaskar Rao DV (2006) The evaluation of Kain–Fritsch scheme in tropical cyclone simulation. Mausam 57:395–410

Skamarock WC, Klemp JB, Dudhia J, Gill DO, Barker DM, Dudha MG, Huang X, Wang W, Powers JG (2008) A description of the advanced research WRF version 3. NCAR technical note NCAR/TN-475+ STR, 113 p. http://www2.mmm.ucar.edu/wrf/users/docs/arw_v3.pdf. Accessed 5 June 2017

Smith RB (1993) A hurricane beta-drift law. J Atmos Sci 50:3213–3215

Srinivas CV, Bhaskar Rao DV, Venkatesan R, Hari Prasad D (2007) Numerical simulation of Andhra severe cyclone (2003): sensitive to the boundary layer and convection parameterization. Pure Appl Geophys 164:23

Srinivas CV, Bhaskar Rao DV, Yesubabu Y, Baskaran R, Venkatraman B (2013) Tropical cyclone predictions over the Bay of Bengal using the high-resolution advanced research weather research and forecasting (ARW) model. Q J R Meteorol Soc 139(676):1810–1825

Takahashi T (1978) Riming electrification as a charge generation mechanism in thunderstorms. J Atmos Sci 35:1536–1548

Velden CS, Leslie LM (1991) The basic relationship between tropical cyclone intensity and the depth of the environmental steering layer in the Australian region. Wea Forecast 6:244–253

Wang B, Li X (1992) The beta drift of three dimensional vortices: a numerical study. Mon Wea Rev 120:579–593